Chapter 6

CONSTRAINT ON CENTRAL DARK MATTER DENSITY IN THE EDDINGTON INSPIRED BORN-INFELD (EiBI) GRAVITY.

6.1 Introduction

The proportional relation between the stress-energy tensor and the geometry in general relativity is an effect of the coupling between matter and gravity. This matter-gravity coupling is linear, in general, though there is no obvious reason behind it. Modified theories of gravity that usually effect the vacuum dynamics are the evidence for the linearity of the matter-gravity coupling [1, 2]. Based on Eddington gravity action [3] and Born-Infeld nonlinear electrodynamics [4], Eddington-inspired Born-Infeld (EiBI) theory has been proposed [5] recently to provide matter-gravity coupling modifications. This theory agrees with the stable compact pressureless stars coined

by perfect fluid, which opens a new horizon of self-gravitating dark matter.

The impact of positive coupling parameters on the collapse of dust and on singularities, optimal constraint on the coupling parameters are elaborated in [6]. The evolution of a homogeneous and isotropic Friedmann-Robertson-Walker universe in the context of the EiBI theory of gravity has been discussed in [7]. Its non-trivial coupling to matter restrain singularities in early cosmology and in the non-relativistic collapse of non-interacting particles. Any positive coupling corresponds to a collapse to pressureless star rather than a singularity. Chandrasekhar limit for the mass of non-relativistic white dwarf does not exist in this theory [8]. The initial state of an anisotropic universe, in this theory, may be regular if the quadratic power for large field value dominates the scalar potential [9]. EiBI theory may be used to avoid cosmological singularities [10]. This theory recalls the Palatini gravity formulation in aspect of curvature singularities at the surface of polytropic stars [11].

To get a more complete view of the EiBI theory and the Weyl gravity, it is necessary to mention that several important predictions follow from the two theories. For instance, recent investigation by Du et al. [12] on large scale structure formation in the EiBI gravity shows a deviation in the matter power spectrum between the EiBI gravity and the CDM model, which is a testable prediction. Stability and localization of gravitational fluctuations in the EiBI brane system have been studied in Refs. [13, 14]. Further, as shown by Wei et al. [15], strong gravitational lensing observables in EiBI are controlled by the coupling parameter κ, which is a new prediction that

lends itself to future testing. Similarly, in Weyl gravity, the first order light deflection angle $\theta_{\rm W}$ by a galaxy, first obtained by Edery and Paranjape [16], contains the galactic halo parameter γ appearing in the Mannheim-O'Brien (MO) model. Bhattacharya et al. [17, 18] calculated higher order deflection terms. Strong field lensing in the Weyl gravity has been studied recently in [19], and the predictions can be verified by actual observations in future. A remarkable feature of Weyl gravity is that its solution, the MO model, already contains the successes of the well tested Schwarzschild gravity as a special case. All the above exemplify the current status of the capabilities of the two theories in question.

The possibility of perfect fluid dark matter within the framework of general relativity has already been explored in the literature [20, 21]. A similar possibility has been recently investigated within the framework of the EiBI theory by Harko et al. [22, 23] and this is the model we are going to analyze further in this paper. Using a tangential velocity profile [24, 25] giving Universal Rotation Curves (URC) and setting the cosmological constant to zero, they obtained, in the Newtonian approximation, a new galactic metric and theoretically explored its gravitational properties. However, the numerical values of the crucial parameter κ (denoted by $\kappa = 2R_{DM}^2/\pi^2$) or equivalently the dark matter radius $R_{\rm DM}$, cannot be determined from the theory alone – it has to be obtained either from the observed data or from some other model. It is also expected that the values of $R_{\rm DM}$ would differ from galaxy to galaxy. On the other hand, to our knowledge, apart from the observed last scattering radii $R_{\rm last}$, the

astrophysical literature still seems to lack concrete observed data on $R_{\rm DM}$ for individual galaxies. Therefore, an appropriate numerical input for $R_{\rm DM}$ is needed, which we take from Weyl gravity, if we want to make quantitative predictions.

At this point, we recall a novel idea of Edery & Paranjape [16], where they bridged two different metric theories by equating the same Einstein angle $\theta_{\rm E}$ (caused by the luminous + dark matter) with the Weyl angle $\theta_{\rm W}$ (caused by the luminous matter alone), and drew useful and testable conclusions using the identity $\theta_{\rm E} = \theta_{\rm W}$. Motivated exactly by this idea, we equate the same EiBI radius of dark matter $R_{\rm DM}$ (caused by dark matter source) with the geometric Weyl radius of the galactic halo $R_{\rm WR}$ (caused by the luminous matter alone). With the numerical input $R_{\rm DM} = R_{\rm WR}$, we shall quantify the relevant central densities in the EiBI theory. We wish to clarify that we are not talking here of merging or mapping the two theories into one another per se but concentrating only on a particular common prediction. The theories are of course different from each other – one with dark matter source and the other without, not to mention differences elsewhere. But both are metric theories capable of predicting for any given galactic sample with a dark matter/halo boundary arising out of the same stability condition $V'' < 0$ (as used, e.g., in the braneworld dark matter [26]). Therefore, without any bias to either theories, we shall investigate if this input leads to limits on dark matter central density ρ_0 consistent with those estimated from fits to different known profiles. We shall see that it does.

The radius $R_{\rm WR}$ is to be understood as the geometric halo radius with its interior

being filled with Weyl vacuum [1]. We stress that Weyl vacuum is not a vacuum in the ordinary sense but an arena of interplay of several potential energies, predominantly the global quadratic potential due to cosmic inhomogeneities [27]. Thus, our input physically means that the total potential energy contained within the halo radius $R_{\rm WR}$ of Weyl gravity equals the total invisible dark matter energy contained within $R_{\rm DM}$ of EiBI gravity. The radius $R_{\rm DM}$ is defined by the absence of dark matter density at the halo boundary [22, 23], while $R_{\rm WR}$ is defined by the absence of stable circular orbits at the halo boundary [28]. Since stability is an essential physical criterion because Doppler emissions from the halo emanate from stable circular orbits of hydrogen gas [29], we think that $R_{\rm WR}$ should be regarded as the only testable upper limit on the radius of a galactic halo. Fortunately, observed last scattering data $R_{\rm last}$ so far have not surpassed the predicted limiting value $R_{\rm WR}$ for all the galaxies studied to date, thereby lending excellent observational support to the MO model prediction of $R_{\rm WR}$.

6.2 Outline of the EiBI halo model

EiBI theory is governed by the gravitational action $\mathrm{S}_{\mathrm{Ei}\,BI}$, given by [5, 22]

$$S_{\mathrm{Ei}\,BI} = \frac{1}{16\pi}\frac{2}{\kappa}\int d^4x[\sqrt{-\mid g_{\mu\nu} + 8\pi\kappa R_{\mu\nu}\mid} - \lambda\sqrt{-g}] + S_M[g, \Psi_M], \tag{6.1}$$

with $\lambda \neq 0$ is a dimensionless parameter, $g_{\mu\nu}$ is the physical metric, κ is a parameter with inverse dimension to that of the cosmological constant Λ and $R_{\mu\nu}$ is the sym-

[1]Note that we are using here the terminology $R_{\rm WR}$ in lieu of $R^{\rm max}_{\rm stable}$ of Ref.[28] only to bring it in line with the notation of the present analysis.

metric part of the Ricci tensor and is derived from $\Gamma^{\alpha}_{\beta\gamma}$. The matter action S_M is a function of the matter fields Ψ_M and $g_{\mu\nu}$. $\mid g_{\mu\nu}+8\pi\kappa R_{\mu\nu} \mid$ denotes the determinant of $g_{\mu\nu}+8\pi\kappa R_{\mu\nu}$. For small values of κR, the action (6.1) reproduces the Einstein-Hilbert action with $\lambda = \kappa\Lambda + 1$, where Λ is the cosmological constant, while for large values of κR, this action approximates to that of Eddington, viz., $S_{\rm Edd} = 2\kappa \int d^4x[\sqrt{\mid R \mid}$. For more details, see [30, 31].

Harko et al. [22, 23] deals with dark matter modeling assuming certain restrictive conditions such as spherical symmetry and asymptotic flatness, the latter requiring that $\Lambda = 0 \Leftrightarrow \lambda = 1$. These assumptions of course limit the applicability of EiBI theory but makes the problem at hand much simpler to handle. Therefore, the characteristics of various cosmological and stellar scenarios that can be govern by that action $S_{{\rm Ei}\,BI}$, are determined by the remaining parameter κ. For instance, the critical mass (above which pressureless compact objects may collapse into a black hole) is approximately equal to $\kappa^{1/2}c^2G^{3/2}$ and the maximum density that the matter inside of a stable compact star can attain is nearly equal to c^2/κ. For a gravitationally bound astrophysical objects of size R, $\kappa < GR^2$ [32]. Several constrain for κ with a three dimensional EiBI gravity is studied in [33].

There are two metrics in the EiBI theory, namely, the physical metric ($g_{\mu\nu}$) and the auxiliary metric ($q_{\mu\nu}$) which are connected by the field equations [22]

$$q_{\mu\nu} = g_{\mu\nu} + 8\pi\kappa R_{\mu\nu}, \tag{6.2}$$

$$q^{\mu\nu} = \tau(g^{\mu\nu} + 8\pi\kappa T^{\mu\nu}), \tag{6.3}$$

yield by varying the action (6.1) with respect to the connection $\Gamma^{\alpha}_{\beta\gamma}$ and with respect to the real metric $g_{\mu\nu}$, respectively. The auxiliary metric $q_{\mu\nu}$ is related to the connection $\Gamma^{\alpha}_{\beta\gamma}$ by

$$\Gamma^{\alpha}_{\beta\gamma} = \frac{1}{2}q^{\alpha\sigma}(\partial_{\gamma}q_{\sigma\beta} + \partial_{\beta}q_{\sigma\gamma} - \partial_{\sigma}q_{\beta\gamma}),$$

and τ is defined as $\tau = \sqrt{g/q}$. In vacuum where the stress-energy tensor $T^{\mu\nu}$ vanishes, we have $q_{\mu\nu} = g_{\mu\nu}$ (from Eq.(6.2)), i.e. EiBI theory is equivalent to standard general relativity.

The line elements, corresponding to both the metrics, representing a static and spherically symmetric dark matter halo is of the form [22]

$$g_{\mu\nu}dx^{\mu}dx^{\nu} = -e^{\nu(r)}dt^2 + e^{\lambda(r)}dr^2 + f(r)(d\theta^2 + \sin^2\theta d\phi^2), \tag{6.4}$$

$$q_{\mu\nu}dx^{\mu}dx^{\nu} = -e^{\beta(r)}dt^2 + e^{\alpha(r)}dr^2 + r^2(d\theta^2 + \sin^2\theta d\phi^2), \tag{6.5}$$

respectively where $\nu(r)$, $\lambda(r)$, $f(r)$, $\beta(r)$ and $\alpha(r)$ are arbitrary metric functions of the radial coordinate r. The galactic halo is assumed to be filled with perfect fluid dark matter with energy-momentum tensor $T^{\mu\nu} = (p+\ \rho)U^{\mu}U^{\nu} + pg^{\mu\nu}$ where ρ is the energy density, p is the isotropic pressure and U^{μ} is the four velocity of the fluid satisfying $g_{\mu\nu}U^{\mu}U^{\nu} = -1$, then the system of gravitational field equations assent that [22]

$$\frac{d}{dr}(re^{-\alpha}) = 1 - \frac{1}{2\kappa}(2 + \frac{a}{b^3} - \frac{3}{ab})r^2, \tag{6.6}$$

$$e^{-\alpha}(1 + r\frac{d\beta}{dr}) = 1 + \frac{1}{2\kappa}(\frac{1}{ab} + \frac{a}{b^3} - 2)r^2, \tag{6.7}$$

$$e^{\beta} = \frac{e^{\nu}b^3}{a},\ e^{\alpha} = e^{\lambda}ab,\ f = \frac{r^2}{ab}, \tag{6.8}$$

where $a = \sqrt{1 + 8\pi\kappa\rho}$ and $b = \sqrt{1 - 8\pi\kappa p}$.

Let us consider the tangential velocity profile provided by the Universal Rotation Curve (URC) [24, 25]

$$v_{tg}^2 = v_\infty^2 \frac{(r/r_{opt})^2}{r_0^2 + (r/r_{opt})^2}, \tag{6.9}$$

where r_{opt} is the optical radius containing 83% of the galactic luminosity. The parameter r_0 is the halo core radius in units of r_{opt} and the asymptotic velocity(v_∞) is given by $v_\infty^2 = v_{opt}^2(1-\beta_*)(1+r_0^2)$ where $v_{opt} = v_{tg}(r_{opt})$, $\beta_* = 0.72 + 0.44 Log_{10}[L/L_*]$ and $L_* = 10^{10.4} L_\odot$. For spiral galaxies $r_0 = 1.5(L/L_*)^{1/5}$. If $r \to 0$, $v_{tg} \to 0$ and $v_{tg} \to v_\infty$ for $r/r_{opt} \gg r_0$. The expression of $v_{\rm tg}^2$ for a test particle in a stable circular orbit is $v_{\rm tg}^2 = r\nu'/2$ [22]. Therefore, the general static and spherically symmetric metric of the dark matter halo takes the form

$$d\tau^2 = -e^{\nu_0}[(\frac{r}{r_{opt}})^2 + r_0^2]^{v_\infty^2} dt^2 + e^{\lambda(r)} dr^2 + r^2(d\theta^2 + \sin^2\theta d\phi^2), \tag{6.10}$$

where e^{ν_0} is an arbitrary constant of integration.

Let us consider that the motion of the massive test particles in EiBI gravity take place in a pressureless cosmic medium i.e. $8\pi\kappa p \ll 1$ and the density of the dark matter is small i.e. $8\pi\kappa\rho \ll 1$. Then, to a first order of the coupling constant κ, the differential equation describing the dark matter profile in EiBI gravity can be obtained as [22]

$$\frac{1}{r^2}\frac{d}{dr}(r^2\frac{d\rho}{dr}) + \frac{2}{\kappa}\rho = 16\pi\rho\rho' r. \tag{6.11}$$

To obtain an approximate solution of Eq.(6.11), we can neglect the non-linear

term containing ρ i.e. $16\pi\rho\rho^{'}r$ at the right hand side of it. Thus, Eq.(6.11) simplifies to [22]

$$\frac{1}{r^2}\frac{d}{dr}(r^2\frac{d\rho^{(0)}}{dr})+\frac{2}{\kappa}\rho^{(0)}=0, \tag{6.12}$$

which is the Lane-Emden equation for the polytropic index $n=1$ [34, 35]. Thus with the assumptions that $8\pi\kappa p \ll 1$ and that the velocity of the test particles in circular stable orbits around the galactic center is constant, a first order approximation of the coupling constant κ yield a dark matter density profile which satisfy the Lane-Emden equation with a polytropic index $n=1$.

A non-singular solution of the Eq.(6.12) at the center is given by [22]

$$\rho^{(0)}(r)=K\frac{\mathrm{Si}\,n(\sqrt{\frac{2}{\kappa}}r)}{\sqrt{\frac{2}{\kappa}}r}, \tag{6.13}$$

where K is an arbitrary constant of integration. At the center of the galactic halo $\rho^{(0)}(0)=\rho_0$, the central dark matter density. Therefore from Eq.(6.13), $K=\rho_0$. Assuming that the halo has a sharp boundary R_{DM}, where the density vanishes i.e. $\rho^{(0)}(R_{DM})=0$. Thus, from Eq.(6.13), we can obtain $R_{DM}=\sqrt{\frac{\kappa}{2}}\pi$. The density profile (6.13) exhibits an unphysical behavior of becoming negative for $R_{DM}<R<2R_{DM}$, which is why one has to require a sharp halo boundary $\rho^{(0)}(R\geq R_{DM})=0$. This quite specific behavior of the density profile differs from those of Navarro-Frenk-White (NFW) or Burkert density profiles (that decay to zero only as $r\to\infty$)[36].

The mass profile of the dark matter, $M(r)=4\pi\int_0^r\rho^{(0)}(r)r^2dr$, is given by

$$M(\bar{r})=\frac{4R_{DM}^3\rho_0}{\pi^2}[\sin(\bar{r})-\bar{r}\cos(\bar{r})], \tag{6.14}$$

where $\bar{r} = \pi r/R_{DM}$.

Again, the q-metric coefficient e^{α} can be obtained as [22]

$$e^{-\alpha} = 1 - \frac{2M(r)}{r} = 1 - \frac{\bar{\rho}_0}{\bar{r}}[\sin(\bar{r}) - \bar{r}\cos(\bar{r})]. \tag{6.15}$$

and the g-metric coefficients are given by

$$e^{-\lambda} = e^{-\alpha}a = e^{-\alpha}[1 + \frac{\bar{\rho}_0}{\bar{r}}\sin(\bar{r})], \tag{6.16}$$

$$f(\bar{r}) = \frac{(R_{DM}^2/\pi^2)\bar{r}^2}{\sqrt{1+8\pi\kappa\rho}} = \frac{R_{DM}^2\bar{r}^2}{\pi^2}[1 - \frac{\bar{\rho}_0}{\bar{r}}\sin(\bar{r})], \tag{6.17}$$

where $\bar{\rho}_0 = \frac{8R_{DM}^2\rho_0}{\pi}$.

Therefore, with some specified assumptions like $(r/r_{opt})^2 \gg r_0^2$ and $8\pi\kappa p \ll 1$, the dark matter profile (in an exact analytic form) with full galactic dark matter metric, in both g and q geometries, can be obtained. Thus, the governing metric of the dark matter halo became [22]

$$\begin{aligned}
d\tau^2 &= -B(\overline{r})dt^2 + A(\overline{r})d\overline{r}^2 + \overline{r}^2C(\overline{r})(d\theta^2 + \sin^2\theta d\phi^2), \qquad (6.18)\\
B(\overline{r}) &= e^{\nu_0}\left[\left(\frac{R_{\rm DM}}{\pi r_{\rm opt}}\right)^2\overline{r}^2 + r_0^2\right]^{v_\infty^2},\\
A(\overline{r}) &= \left(\frac{R_{\rm DM}}{\pi}\right)^2\frac{1}{\left[1 - \frac{\overline{\rho}_0}{\overline{r}}\sin(\overline{r}) + \overline{\rho}_0\cos(\overline{r})\right]\left[1 - \frac{\overline{\rho}_0}{\overline{r}}\sin(\overline{r})\right]},\\
C(\overline{r}) &= \left(\frac{R_{\rm DM}}{\pi}\right)^2\left[1 - \frac{\overline{\rho}_0}{\overline{r}}\sin(\overline{r})\right].
\end{aligned}$$

Total mass of the dark matter halo contained in the spherical region of radius R_{DM} is (from Eq.(6.14))

$$M_{DM} = M(R_{DM}) = \sqrt{2}\pi^2\kappa^{3/2}\rho_0 = \frac{4}{\pi}\rho_0 R_{DM}^3. \tag{6.19}$$

The mean density of the dark matter halo is defined as

$$\langle\rho\rangle \ = \frac{M_{DM}}{4\pi R_{DM}^3/3} = \frac{3\rho_0}{\pi^2}. \tag{6.20}$$

Note that the surface area of a sphere at the boundary of dark matter halo defined by $\bar{r} = \pi$, has the value $S = 4\pi\frac{R_{DM}^2\bar{r}^2}{\pi^2} = 4\pi R_{DM}^2$, which is just the spherical surface area in "standard coordinates". Thus the dark matter radius R_{DM} can be identified with standard coordinate halo radius R_{WR} derived below. We shall need some of the above equations in the sequel.

6.3 Outline of the Mannheim-O'Brien conformal gravity model

The unique Weyl action is

$$\begin{aligned} S_{\rm Weyl} &= -\alpha_{\rm g}\int d^4x\sqrt{-g}\left[C_{\lambda\mu\nu\sigma}C^{\lambda\mu\nu\sigma}\right] \\ &= -2\alpha_{\rm g}\int d^4x\sqrt{-g}\left[R_{\mu\sigma}R^{\mu\sigma} - \frac{1}{3}\left(R^{\alpha}_{\alpha}\right)^2\right], \end{aligned} \tag{6.21}$$

where $C^{\lambda\mu\nu\sigma}$ is the Weyl tensor and $\alpha_{\rm g}$ is the dimensionless gravitational constant. The metric ansatz in standard coordinates taken in [27] is

$$d\tau^2 = -B(r)dt^2 + \frac{1}{B(r)}dr^2 + r^2(d\theta^2 + \sin^2\theta d\phi^2). \tag{6.22}$$

With this ansatz, the geodesic for a single test particle yields the tangential velocity of material circular orbits at the arbitrary radius $r = R$ as [37]

$$v_{\rm tg}^2 = \left(Rc^2/2\right)B', \tag{6.23}$$

where prime denotes derivative with respect to R.

In Weyl gravity, a given local gravitational source generates a gravitational potential per unit solar mass as follows (Eq.(8) of Ref. [37]): $V^*(r) = -\frac{\beta^* c^2}{r} + \frac{\gamma^* c^2 r}{2}$ where β^* and γ^* are constants. Integrating V^* over the luminous matter distribution in the Weyl gravity, Mannheim [37, 38] obtained to a good approximation the following expression of the local contribution to the centripetal acceleration suffered by a test particle in circular orbit at $R > 4R_0$:

$$\frac{v_{\rm LOC}^2}{R} \simeq \frac{N^*\beta^* c^2}{R^2}\left(1 - \frac{9R_0^2}{2R^2}\right) + \frac{N^*\gamma^* c^2}{2}\left(1 - \frac{3R_0^2}{2R^2} - \frac{45R_0^4}{8R^4}\right). \qquad (6.24)$$

The meanings and values of the symbols above are as follows: R_0 is the scale length such that most of the surface brightness is contained in $R \leq 4R_0$ of the optical disk region. From the observed galactic mass-to-light ratio (M/L), one can define the total number of solar mass units N^* in the galaxy via $(M/L)L = M_{\rm lum} = N^* M_\odot$. The values of the constants giving best fits to rotation curves of all the 111 galaxy samples in [37] are:

$$\begin{aligned} \beta^* &= GM_\odot/c^2 = 1.48 \times 10^5 \text{ cm}, \gamma^* = 5.42 \times 10^{-41} \text{ cm}^{-1}, \\ \gamma_0 &= 3.06 \times 10^{-30} \text{ cm}^{-1}, k = 9.54 \times 10^{-54} \text{ cm}^{-2}. \end{aligned} \qquad (6.25)$$

Adding to Eq.(6.24) two more components, Mannheim [37] proposed the complete

expression

$$\begin{aligned}\frac{v_{\rm tg}^2}{R} &= \frac{v_{\rm LOC}^2}{R}+\frac{\gamma_0 c^2}{2}-kc^2R \\ &= \frac{N^*\beta^* c^2}{R^2}\left(1-\frac{9R_0^2}{2R^2}\right)+\frac{N^*\gamma^* c^2}{2}\left(1-\frac{3R_0^2}{2R^2}-\frac{45R_0^4}{8R^4}\right) \\ &\quad +\frac{\gamma_0 c^2}{2}-kc^2R, \end{aligned} \tag{6.26}$$

with the asymptotic limit

$$\frac{v_{\rm tg}^2}{R}\rightarrow\frac{N^*\beta^* c^2}{R^2}+\frac{N^*\gamma^* c^2}{2}+\frac{\gamma_0 c^2}{2}-kc^2R, \tag{6.27}$$

where one recognizes the Schwarzschild-like potential $V_{\beta^*}=N^*\beta^*c^2/R$, two linear potential terms, viz., a local $V_{\gamma^*}=N^*\gamma^*c^2R/2$ associated with the matter distribution within a galaxy and a global $V_{\gamma_0}=\gamma_0 c^2R/2$ associated with the cosmological background, while the universal de Sitter-like quadratic potential term $V_k=-kc^2R^2$ is induced by inhomogeneities in the cosmic background. Note that the last three potentials are new inputs into the MO model [27] designed to interpret the rotation curve data. It is evident from Eq.(6.26) that, in making the fits, the *only one* parameter that can vary from one galaxy to the other is the ratio (M/L) leading to a galaxy dependent N^*. The known HI gas mass is included in the fit. With everything else being universal, no dark matter is needed; the metric effect is enough to account for the observed rotation data. This is the so-called "no-dark-matter" paradigm underlying the MO model.

For each galaxy with specific value of N^* and other fixed constants as in (6.25), $v_{\rm tg}^2$ of Eq.(6.26) gives a *finite* value of R at the terminating velocity $v_{\rm tg}^2(R_{\rm term})=0$.

To illustrate various results derived here, we need to consider samples and so in the following we choose the LSB galactic sample ESO 1200211. The plot in Figure 6.1 shows that the rotation curve $v_{\rm tg}^2$ decays to zero at a radial distance $R_{\rm term} = 52.04$ kpc [36], but this is still not the halo radius. The actual halo radius $R_{\rm WR}$ will always be less than the value of $R_{\rm term}$ for reasons of stability, as worked out below.

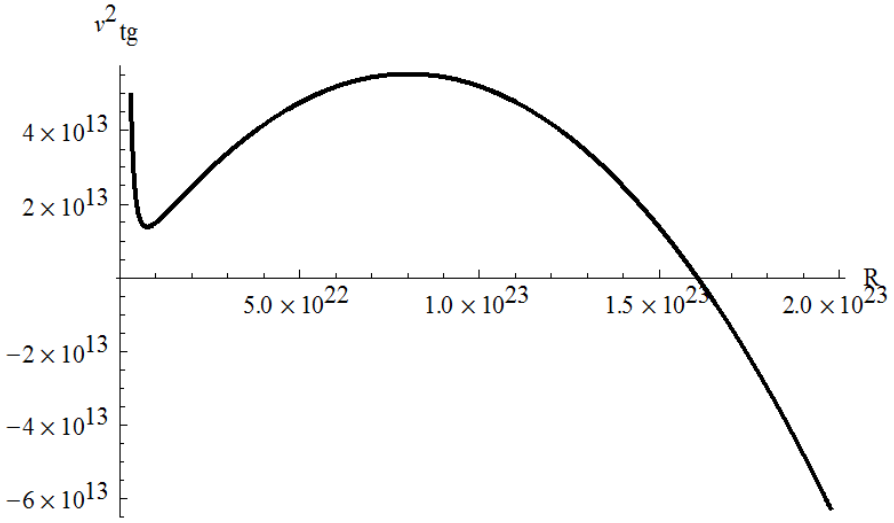

Figure 6.1. Plot of $v_{\rm tg}^2$ vs R (cm) using Eq.(6.26) for ESO 1200211. The luminous mass is $M_{\rm lum} = 5.6 \times 10^7 M_\odot$ so that $N^* = 5.6 \times 10^7$. The other constants are in (6.25) and $R_0 = 2$ kpc [37]. One finds the velocity terminating radius $R_{\rm term} = 52.04$ kpc.

Using Eq.(6.26) in Eq.(6.23) and integrating, we get

$$B(R) = 1 - \frac{2N^*\beta^*}{R} + (N^*\gamma^* + \gamma_0)\,R - kR^2 + \frac{3R_0^2 N^*\gamma^*}{2R} + \frac{15R_0^4 N^*\gamma^* - 24R_0^2 N^*\beta^*}{8R^3}. \quad (6.28)$$

The metric function $B(R)$ has a term proportional to k that corresponds to the so called quadratic potential $V_k(R) = -kc^2R^2$ used in [27]. The radial geodesic in the metric (6.22) is given by

$$\left(\frac{dr}{dt}\right)^2 = B^2(r) - a\frac{B^3(r)}{r^2} - bB^3(r), \quad (6.29)$$

where a and b are constants of motion. The right hand side of the above equation is the "effective potential" V, and $V''_{\rm MO} \equiv f(R)$ involves the derivatives of $B(R)$ containing that quadratic potential.

The presence of this quadratic component V_k via $B(R)$ in the $f(R)$ produces a finite $R_{\rm WR}$, as explained in Ref.[28]. The crucial importance of V_k is that if it is absent in $B(R)$, there would be no finite terminating value for $R_{\rm WR}$. The main reason is the negative sign in V_k needed for the data fit by MO. Because of this, it is quite evident from the plot of $V''_{\rm MO}$ (Figure 6.2) that the sample ESO 1200211 has a maximally allowed finite halo radius ~ 39.033 kpc. On the other hand, if V_k has a positive sign (in which case no fit to data) or is altogether removed from $B(R)$, hence from $V''_{\rm MO}$, it can be graphically verified that there will be no finite stable radius $R_{\rm WR}$ for the halo. This shows the crucial role of V_k. Thus, it is the requirement of fitting to data that indirectly limits the halo size to $R_{\rm WR}$. As to the physical reason, we see that

the repulsive potential V_k balances the remaining attractive potentials at $r = R_{\rm term}$ [see Eq. (6.27)] but stability further demands that $R_{\rm WR} < R_{\rm term}$, as is evident from Figures 6.1 & 6.2. Therefore, we can say that, at $r = R_{\rm WR}$, attractive potentials prevail over the repulsive potential V_k constraining the gas on the circular orbit, as it should.

The right hand side of Eq.(6.29) and its first derivative with respect to r, both must vanish at the circular radius $r = R$ giving

$$a = \frac{R^3 B'(R)}{2B^2(R)}, \quad b = \frac{2B(R) - RB'(R)}{2B^2(R)}. \tag{6.30}$$

The condition for stability is that the second derivative of the "effective potential" V with respect to r must be negative at the circular radius $r = R$. The resultant expression with values of a, b plugged in leads to the generic stability criterion for the MO model:

$$V''_{\rm MO} = 2B'^2(R) - B(R)B''(R) - 3B(R)B'(R)/R < 0. \tag{6.31}$$

This inequality graphically predicts a finite, stable, maximum halo radius that we call $R_{\rm WR}$ caused solely by the quadratic potential $V_k(R) = -kc^2R^2$. Interestingly, the predicted $R_{\rm WR}$ lends itself to observational testing in the near future as its value does not often much exceed the $R_{\rm last}$ for many samples.

The above algorithm is applicable to all the 111 galaxy samples but for illustration, we display $V''_{\rm MO}$ *vs* R for the same sample ESO 1200211 in Figure 6.2. The value of N^* can be found from $N^* = M_{\rm lum}/\beta^*$, where $M_{\rm lum} = [(M/L)_{\rm stars} \times L_{\rm B} + M_{\rm HI}] \times 10^{10} M_\odot$.

All necessary components can be read off from the entries in the *Table IV* in [37]. The value of N^* $(= 5.60 \times 10^7)$ together with other constants in (6.25), when plugged into the inequality (6.31), immediately graphically yields $R = R_{\rm WR} = 39.03$ kpc [36], which is less than $R_{\rm term}$ calculated above.

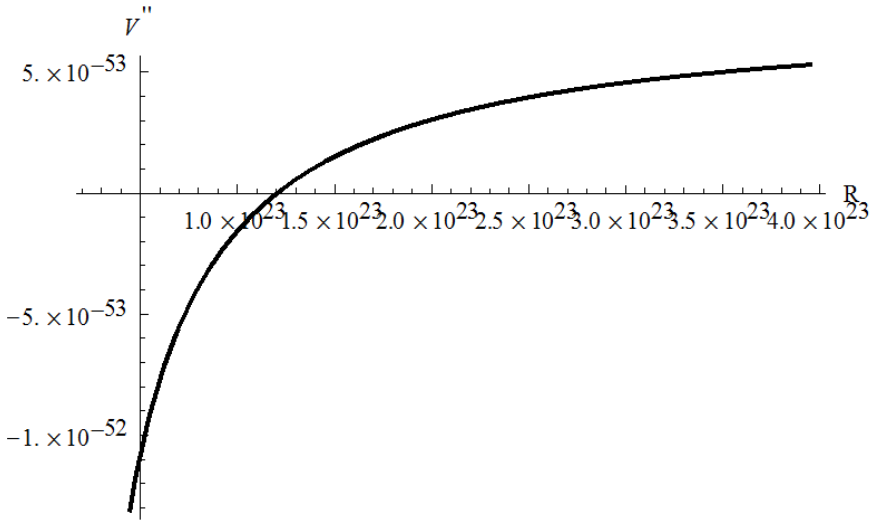

Figure 6.2. Plot of V'' vs R (cm) using Eq.(6.31). The crossing shows the halo radius $R_{\rm WR} = 39.03$ kpc ($\equiv 1.204 \times 10^{23}$ cm), which is the maximally allowed radius supporting stable circular orbits in the halo of ESO 1200211, for which $R_0 = 2$ kpc. The plot is made for the radii $R > 4R_0$.

6.4 Upper limit on density for stability

To analyze the stability of circular orbits, one needs to analyze the second order derivative of the concerned potential, which we wish to do here. To find the potential V, note that the four velocity $U^\alpha = \frac{dx^\alpha}{d\tau}$ of a test particle of rest mass m_0 moving in the halo (restricting ourselves to $\theta = \pi/2$) follows the equation $g_{\nu\sigma}U^\nu U^\sigma = -m_0^2$ that can be cast into a Newtonian form in the dimensionless radial variable $\overline{r}$ $(= \pi r/R_{\rm DM})$ as

$$\left(\frac{d\overline{r}}{d\tau}\right)^2 = E^2 + V_{\rm EiBI}(\overline{r}), \tag{6.32}$$

which gives, for the metric Eq.(6.18), the EiBI potential [36]

$$V_{\rm EiBI}(\overline{r}) = \left[E^2\left\{\frac{1}{AB} - 1\right\} - \frac{L^2}{AC\overline{r}^2} - \frac{1}{A}\right], \tag{6.33}$$

$$E = \frac{U_0}{m_0},\ L = \frac{U_3}{m_0}, \tag{6.34}$$

where the constants E and L, respectively, are the conserved relativistic energy and angular momentum per unit mass of the test particle. Circular orbits at any arbitrary radius are defined by $\overline{r} = \overline{R} =$ constant, so that $\frac{d\overline{r}}{d\tau}\ |_{\overline{r}=\overline{R}} = 0$ and, additionally, $\frac{dV}{d\overline{r}}\ |_{\overline{r}=\overline{R}} = 0$. From these two conditions follow the conserved quantities as under [36]:

$$L^2 = \frac{X}{Z}, \tag{6.35}$$

and using it in $V_{\rm EiBI}(\overline{R}) = -E^2$, we get

$$E^2 = \frac{Y}{Z}, \tag{6.36}$$

where

$$X \equiv -\kappa^2 \overline{R}^3 v_\infty^2 (\overline{R} - \overline{\rho}_0 \sin \overline{R})^2, \tag{6.37}$$

$$Y \equiv \left(\kappa \overline{R}^2 + 2r_0^2 r_{\rm opt}^2\right) \left(r_0^2 + \frac{\kappa \overline{R}^2}{2r_{\rm opt}^2}\right)^{v_\infty^2} \left(\overline{\rho}_0 \overline{R} \cos \overline{R} + \overline{\rho}_0 \sin \overline{R} - 2\overline{R}\right), \tag{6.38}$$

$$\begin{aligned} Z \equiv & \left\{\kappa \overline{R}^2 \left(1 - 2v_\infty^2\right) + 2r_0^2 r_{\rm opt}^2\right\} \overline{\rho}_0 \sin \overline{R} + \left(\kappa \overline{R}^2 + 2r_0^2 r_{\rm opt}^2\right) \overline{\rho}_0 \overline{R} \cos \overline{R} \\ & -4\overline{R} r_0^2 r_{\rm opt}^2 - 2\kappa \overline{R}^3 \left(1 - v_\infty^2\right). \end{aligned} \tag{6.39}$$

Putting the expressions for L^2 and E^2 in Eq.(6.33), we find the complete expression for $V_{\rm EiBI}$. The orbits will be stable if $V''_{\rm EiBI} \equiv \frac{d^2V}{d\overline{r}^2} \mid_{\overline{r}=\overline{R}} < 0$ and unstable if $V''_{\rm EiBI} > 0$. The expression for $V''_{\rm EiBI}$ is [36]

$$\begin{aligned} & V''_{\rm EiBI}\left(\overline{R}; \kappa, \overline{\rho}_0, r_0, r_{\rm opt}, v_\infty\right) \\ = & \left[\frac{2v_\infty^2 \left(\overline{R} + \overline{\rho}_0 \overline{R} \cos \overline{R} - \overline{\rho}_0 \sin \overline{R}\right)}{\overline{R}^2 \left(\kappa \overline{R}^2 + 2r_0^2 r_{\rm opt}^2\right) Z}\right] \times \\ & \Big[32\overline{R}^2 r_0^2 r_{\rm opt}^2 + 8\kappa \overline{R}^4 \left(1 - v_\infty^2\right) + 6\overline{\rho}_0^2 r_0^2 r_{\rm opt}^2 \left(1 + \overline{R}^2\right) \\ & + \kappa \overline{\rho}_0^2 \overline{R}^2 \left(1 - 2v_\infty^2 + 3\overline{R}^2\right) \\ & - 2\overline{R}^2 \left\{14 r_0^2 r_{\rm opt}^2 + \kappa \overline{R}^2 \left(5 - 2v_\infty^2\right)\right\} \overline{\rho}_0 \cos \overline{R} \\ & + \left\{2\left(\overline{R}^2 - 3\right) r_0^2 r_{\rm opt}^2 - \kappa \overline{R}^2 \left(1 - 2v_\infty^2 - \overline{R}^2\right)\right\} \overline{\rho}_0^2 \cos\left(2\overline{R}\right) \\ & - \left\{36 r_0^2 r_{\rm opt}^2 + 4\overline{R}^2 r_0^2 r_{\rm opt}^2 + 6\kappa \overline{R}^2 + 2\kappa \overline{R}^4 - 12\kappa \overline{R}^2 v_\infty^2\right\} \overline{\rho}_0 \overline{R} \sin \overline{R} \\ & + \left\{6 r_0^2 r_{\rm opt}^2 + \kappa \overline{R}^2 - 2\kappa \overline{R}^2 v_\infty^2\right\} \overline{\rho}_0^2 \overline{R} \sin\left(2\overline{R}\right)\Big]. \end{aligned} \tag{6.40}$$

It will be an exaggeration to straightforwardly draw any conclusion about stability or otherwise of the circular orbits. Clearly, much will depend on the parameter

ranges chosen on the basis of physical considerations. While other parameters can be reasonably assigned, the as yet unknown parameters are the dark matter radius κ ($= 2R_{\rm DM}^2/\pi^2$) and the dimensionless central density $\overline{\rho}_0$ ($= 8\rho_0 R_{\rm DM}^2/\pi$), again depending only on κ. In the first order approximation, the density distribution in the dark matter has been assumed in [22] to be low such that $8\pi G\kappa\rho^{(0)}/c^4 \ll 1$, but the central density ρ_0 could still be large since $|\sin(x)/x| \leq 1$ (see Eq.(6.13)). The question therefore is how large or small could it be, or turning it around, could there be any upper limit on ρ_0 imposed by the stability criterion?

The answer is in the affirmative and can be found graphically. It can be found that V'' is indeed very sensitive to changes in ρ_0 leading to different upper limits $\rho_0^{\rm upper}$ for different galactic samples such that stable circular orbits are possible only when $\rho_0 \leq \rho_0^{\rm upper}$. The reason is that $R_{\rm DM}$ changes from sample to sample, as it should, and thereby leads to different (though not too different) values for κ and $\rho_0^{\rm upper}$. Let us again consider the previous sample ESO 1200211, a low surface brightness galaxy with a halo/dark matter radius $R_{\rm WR} \equiv R_{\rm DM} = 39.03$ kpc that corresponds to $\kappa = 308.74$ kpc^2. With κ thus fixed, the other parameters can be fixed respecting the Newtonian approximation, e.g., $r_0 = 0.61$, $v_\infty^2 = 0.000001$, $r_{\rm opt} = 8$ kpc, with the dimensionless radius $\overline{R}$ ($= \pi R/R_{\rm DM}$) chosen in the range $\overline{R} \in [0.5\pi, \pi]$ corresponding to coordinate radii $R \in$ [19.52 kpc, 39.03 kpc], the dimensionless density parameter chosen in the range $\overline{\rho}_0 \in [0.25\pi,\ 0.8\pi]$ and plot $V''_{\rm EiBI}$ *vs* $\overline{R}$ using the expression (6.40).

Graphical analysis shows that, while $V_{\rm EiBI}$ is not much sensitive to the variation

of the other parameters within the Newtonian approximation, it is *greatly* sensitive to the variation of the remaining parameter ρ_0. Figures 6.3 and 6.4 respectively show that, for values of $\overline{\rho}_0 > 0.94$, there is instability in the entire or partial range of the halo radii $\overline{R}$, while Figure 6.5 indicates that there is an upper limit occurring at $\overline{\rho}_0^{\text{upper}} = 0.94 = \lambda^{\text{upper}}\pi$, where $\lambda^{\text{upper}} = 0.299$, such that for $\overline{\rho}_0 \leq \overline{\rho}_0^{\text{upper}}$, all circular orbits in the entire chosen radial range for $\overline{R}$ are stable [36]. It can be verified that this value of λ^{upper} surprisingly remains the *same* for values for κ across the entire range of 111 samples (some tabulated here), so $\overline{\rho}_0^{\text{upper}}$ is quite a reliable limit.

Rewriting in terms of ρ_0, we have [36]

$$\rho_0^{\text{upper}} = \frac{\overline{\rho}_0^{\text{upper}}\pi}{8R_{\text{DM}}^2} = \frac{\lambda^{\text{upper}}}{4\kappa}. \tag{6.41}$$

This by itself is an interesting prediction of EiBI theory. However, if we want to quantify ρ_0^{upper} for a given galaxy, we need to use the value of R_{DM} but since concrete observed values are yet unavailable, we choose to use the input $R_{\text{DM}} = R_{\text{WR}}$. It turns out that this choice, though not mandatory, works well giving definitive values for ρ_0^{upper} for all samples. Plugging in the values of λ^{upper} and κ, we find that the constraint $\overline{\rho}_0 \leq \overline{\rho}_0^{\text{upper}}$ immediately translates into a generic constraint such that for [36]

$$\rho_0 \leq \rho_0^{\text{upper}}, \tag{6.42}$$

all circular orbits in the chosen range for R are stable. Thus, using the value of κ as above in Eq.(6.41), the sample ESO 1200211 quantitatively yields $\rho_0^{\text{upper}} = 5.04 \times 10^{12}$ $M_\odot \text{kpc}^{-3}$. In general, as long as ρ_0 of any galaxy obeys the stability induced constraint

(6.42), the circular material orbits in the halo region will be stable up to a *maximum* radius $R = R_{\rm WR}$.

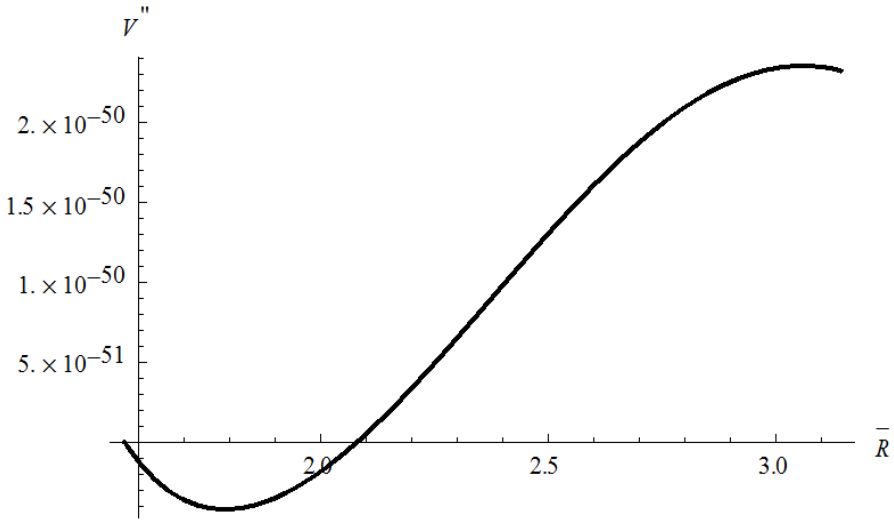

Figure 6.3. Plot of V'' vs $\bar{R} \in [0.5\pi, \pi]$ using Eq.(6.40) for ESO 1200211. The chosen parameters are : $r_0 = 0.61$, $v_\infty^2 = 0.000001$, $r_{opt} = 8$ kpc [$= 2.47 \times 10^{22}$ cm]. Here $\rho_0 = 8.25 \times 10^{12} M_\odot$ kpc^{-3}, which corresponds to $\bar{\rho}_0 = 0.50\pi$. The orbits are unstable in the chosen entire region $\bar{R} \in [0.5\pi, \pi]$ because $V'' > 0$ there.

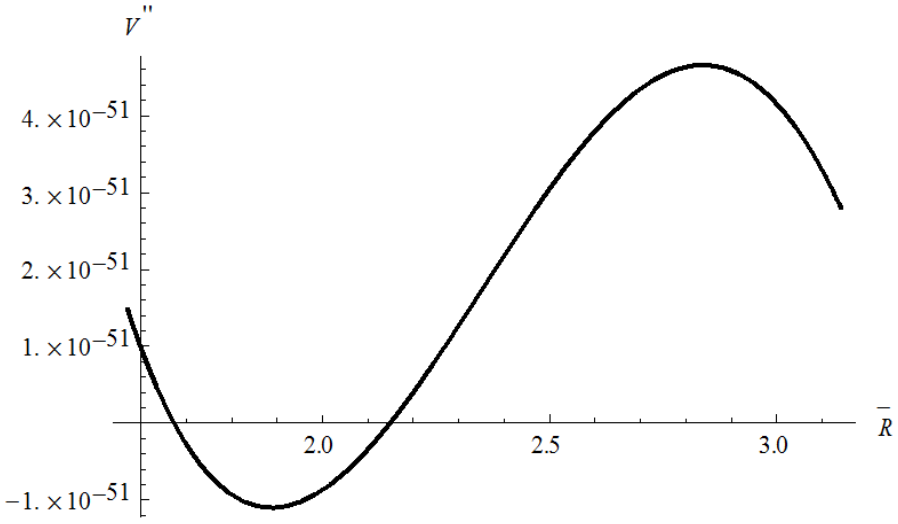

Figure 6.4. Plot of V'' vs $\bar{R} \in [0.5\pi, \pi]$ using Eq.(6.40) for ESO 1200211. The chosen parameters are : $r_0 = 0.61$, $v_\infty^2 = 0.000001$, $r_{opt} = 8$ kpc. Here central density is further lowered to $\rho_0 = 5.61 \times 10^{12} M_\odot$ kpc^{-3}, which corresponds to $\bar{\rho}_0 = 0.34\pi$. The orbits are unstable in some intermediate radii as $V'' > 0$ is partially positive and partially negative.

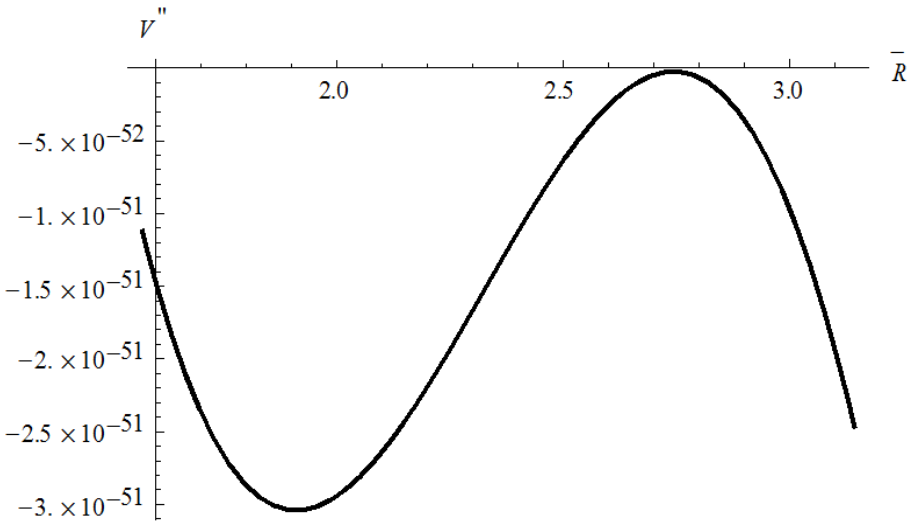

Figure 6.5. Plot of V'' vs $\bar{R} \in [0.5\pi, \pi]$ using Eq.(6.40) for ESO 1200211. The chosen parameters are : $r_0 = 0.61$, $v_\infty^2 = 0.000001$, $r_{opt} = 8$ kpc. Here central density is further lowered to $\rho_0 = 5.04 \times 10^{12} M_\odot$ kpc^{-3}, which corresponds to $\bar{\rho}_0^{upper} = 0.94$. The orbits are stable in the entire chosen region for $\bar{R}$. The corresponding ρ_0 is the upper limit on central density ρ_0^{upper} specific to the sample.

6.5 Central and mean dark matter density

So far, the algorithm has been as follows: Take any galactic sample, find $R_{\rm WR}$ for that sample using the method of the previous section. Then, from the identity $R_{\rm DM} = R_{\rm WR}$, find $R_{\rm DM}$ (hence κ) and using Eq.(6.41), find $\rho_0^{\rm upper}$. However, we still do not know the values of ρ_0 for all the samples observed to date and cannot ascertain whether or not they satisfy the stability induced constraint $\rho_0 \leq \rho_0^{\rm upper}$. On the other hand, some notable dark matter simulations and profiles for several samples show values for ρ_0 that *do* respect this constraint (Table II). This success then prompts us to ask if there is any lower limit on ρ_0 such that $\rho_0^{\rm lower} \leq \rho_0 \leq \rho_0^{\rm upper}$ holds.

Fortunately, there is a way to find the values of $\rho_0^{\rm lower}$, once we are able to estimate the total mass of dark matter $M_{\rm DM}$ using the observed mass-to-light ratios. Fitted data are available for the luminous mass-to-light ratios ($M_{\rm lum}/L_{\rm B}$) in solar units $\Upsilon_\odot$ ($\equiv \frac{M_\odot}{L_\odot}$):

$$\frac{M_{\rm lum}}{L_{\rm B}} = \gamma \Upsilon_\odot.$$

The luminous mass ($M_{\rm lum}$) of a galaxy is contributed mostly by stars and gases excluding dark matter. The stellar mass-to-light ratios γ for 111 samples in [37] are seen to lie between 0.2 and 8 (with just a couple of exceptions), which is consistent with the upper bound of $10\Upsilon_\odot$ suggested by the population synthesis models [39]. On the other hand, there is no detectable dark matter associated with the galactic

disk, most of the dark matter is distributed in the halo [40, 41]. So we can write

$$M_{\rm tot} = M_{\rm lum} + M_{\rm DM}, \tag{6.43}$$

then

$$\frac{M_{\rm tot}}{L_{\rm B}} = \beta \Upsilon_{\odot},$$

where β must be larger than γ, if there is dark matter (observed mass-to-light ratios are still uncertain). We can thus write, following Edery & Paranjape [16]:

$$\frac{M_{\rm lum}}{M_{\rm tot}} = \frac{1}{\alpha}, \tag{6.44}$$

which gives $\beta = \alpha\gamma$ and α should be so chosen as to make $\beta > \gamma$. In general, one takes $\alpha > 1$ such that $M_{\rm tot} > M_{\rm lum}$ thereby accommodating the presence of dark matter.

Assuming that the halos must be substantially larger than the last measured point $R_{\rm last}$, the dark to luminous mass within $R_{\rm last}$ then gives an upper limit of baryon fraction(f_b) through $f_b < \frac{M_{\rm lum}}{M_{\rm tot}}$ and therefore $f_b < \left(1 + \frac{M_{\rm DM}}{M_{\rm lum}}\right)^{-1}$. For some galaxies, $f_b < 0.08$, as reported in de Blok and McGaugh [42]. Thus, using (6.44), we have $f_b < \frac{1}{\alpha}$ and $f_b < 0.08$. Certainly, these inequalities do not constrain α in any way. One of the infinity of options to ensure that both hold simultaneously is to assume that $\frac{1}{\alpha} = 0.08 \Rightarrow \alpha = 12.5$. While α can be varied at will unless it is definitively fixed by independent concrete observed data, we shall for the moment choose the value $\alpha = 12.5$ only to have an idea of the order of magnitudes of the estimated densities, but we shall change α later. The current choice would imply $\beta \in [2.5, 100]$

corresponding to $\gamma \in [0.2, 8]$. The values of $\beta \sim 100$ is enough to account for the large dark matter content of LSB galaxies (i.e., large mass-to-light ratios $\frac{M_{\rm tot}}{L_{\rm B}}$) such as DDO154. Currently favored Burkert density profile can provide an excellent mass model for the dark halos around disk systems up to 100 times more massive than small dwarf galaxies for which the profile was initially intended [43, 44].

The ratio $M_{\rm lum}/M_{\rm tot}$ then gives the connection between $M_{\rm DM}$ of EiBI theory and the luminous mass $M_{\rm lum}$ of galaxies via Eq.(6.43):

$$M_{\rm DM} = (\alpha - 1) M_{\rm lum}. \tag{6.45}$$

Using $R_{\rm WR} \equiv R_{\rm DM}$, Eqs.(6.19) and (6.20) can be rewritten as [36]

$$\rho_0^{\rm lower} = \frac{\pi(\alpha-1)M_{\rm lum}}{4R_{\rm WR}^3}, \quad \langle\rho\rangle^{\rm lower} = \frac{3\rho_0^{\rm lower}}{\pi^2}. \tag{6.46}$$

The superscript "lower" indicates that it is the lower limit of the dark matter central density ρ_0 because $R_{\rm WR}$ is the maximum allowed halo radius (see Figure 6.2), where $V'' < 0$ gives stable radii $R \leq R_{\rm WR}$. Evidently, $\rho_0^{\rm lower}$ is proportional to the as yet unknown parameter α. We are free to raise the value of α arbitrarily, but then the consequent larger values of β would lead to too large an amount of dark matter comparable to that existing in galactic clusters.

To illustrate the order of magnitudes involved for $\rho_0^{\rm lower}$, hence for $\langle\rho\rangle^{\rm lower}$, we again consider the low mass LSB sample ESO 1200211 for which $M_{\rm lum} = 5.60 \times 10^7$ $M_\odot$, $\gamma = 0.2$ and our method, mentioned earlier, yields $R_{\rm WR} = 39.03$ kpc, $\kappa = 308.74$ kpc^2, $R_{\rm term} = 52.04$ kpc. Using Eqs.(6.46), and allowing for a fairly large amount

of dark matter over luminous matter corresponding to $\alpha = 12.5$, we find $\rho_0^{\rm lower} = 8.49 \times 10^4\ M_\odot{\rm kpc}^{-3}$ and $\langle\rho\rangle^{\rm lower} = 2.58 \times 10^4\ M_\odot{\rm kpc}^{-3}$. To compare these values of density, we consider several dark matter density profiles: (i) the Bose-Einstein [45] condensate (ρ_0^{BEC}), (ii) Pseudo-Isothermal [46] profile (ρ_0^{PI}), (iii) the Navarro-Frenk-White [47] profile (ρ_i^{NFW}), (iv) Burkert [43] profile (ρ^{BP}), (see the next section for the exact forms). They yield values as follows: (i) $\rho_0^{BEC} = 1.38 \times 10^7\ M_\odot{\rm kpc}^{-3}$, (ii) $\rho_0^{PI} = 4.64 \times 10^7\ M_\odot{\rm kpc}^{-3}$ and (iii) $\rho_0^{NFW} = 2.45 \times 10^6\ M_\odot{\rm kpc}^{-3}$ for ESO 1200211 (see the entries in *Table I* of [45]). In the previous section, we already found for the present sample the value $\rho_0^{\rm upper} = 5.04 \times 10^{12}\ M_\odot{\rm kpc}^{-3}$. We hence see that $\rho_0^{\rm lower} < \rho_0^{BEC,\ PI\ or\ NFW} < \rho_0^{\rm upper}$ nicely holds. If we take $\alpha < 12.5$, which should also be quite acceptable for many samples, the values of $\rho_0^{\rm lower}$ will only be further lowered and of course the interval will be well supported.

If we increase α to an (unlikely) mammoth value, say $\alpha = 300$ so that $M_{\rm tot} = 300 M_{\rm lum}$ implying $\beta = 60$ so that $\frac{M_{\rm tot}}{L_{\rm B}} = 60\Upsilon_\odot$ in the considered sample, then $\rho_0^{\rm lower} \sim 2.20 \times 10^6\ M_\odot{\rm kpc}^{-3}$, and we notice that the proposed limits are still not violated! If we exclude NFW profile, then the values α can be increased even further. This testifies to the validity of Eqs.(6.46) as well as the limits.

6.6 Testing the limit on the Milky Way

As for our Milky Way galaxy, the latest reported estimates are the following: Using the gas terminal velocity curve, Sgr A* proper motion, an oblate bulge + Miyamoto-

Nagai disc and NFW halo, Kafle *et al.* [48] estimated the luminous (disc + bulge) mass to be $M_{\rm lum} \sim 1.04 \times 10^{11} M_{\odot}$, so that $N^* = 1.04 \times 10^{11}$ and the virial mass inclusive of dark matter $M_{\rm vir} = M_{\rm tot} \sim 0.80 \times 10^{12}\ M_{\odot}$ so that $\alpha = M_{\rm tot}/M_{\rm lum} = 7.68$. (We have not considered the data/fit uncertainties). For alternative but not too different values of $M_{\rm tot}$, see $[49 - 55]$. Using the scale length $R_0 = 4.9$ kpc [48] and the above N^* in the inequality (6.31), we find that $R_{\rm WR} = R_{\rm DM} = 111.90$ kpc. With this value of $R_{\rm WR}$, Eq.(6.41) then yields a value $\rho_{0,\,\rm MW}^{\rm upper} = 6.14 \times 10^{11}\ M_{\odot}{\rm kpc}^{-3}$ characteristic of the Milky way, which does not exceed the maximum density ($\sim 10^{12} M_{\odot}{\rm kpc}^{-3}$) proposed here.

The density profiles considered here are of the forms:

$$\rho^{BP}(r) = \frac{\rho_0^{BP} r_0^3}{(r+r_0)(r^2+r_0^2)} = \rho_0^{BP}\left(1 - \frac{r}{r_0} + \frac{r^4}{r_0^4} + ...\right) \quad [43] \tag{6.47}$$

$$\rho^{NFW}(r) = \frac{\rho_0^{NFW}}{(r/r_S)[1+(r/r_S)^2]} = \rho_0^{NFW}\left(\frac{r_S}{r} - \frac{r}{r_S} + \frac{r^3}{r_S^3} + ...\right) [47] \tag{6.48}$$

$$\rho^{PI}(r) = \frac{\rho_0^{PI}}{1+(r/r_c)^2} = \rho_0^{PI}\left(1 - \frac{r^2}{r_c^2} + \frac{r^4}{r_c^4} + ...\right) \quad [46] \tag{6.49}$$

$$\rho^{BEC}(r) = \rho_0^{BEC}\left[\frac{\sin(\xi r)}{\xi r}\right] = \rho_0^{BEC}\left(1 - \frac{\xi^2 r^2}{6} + \frac{\xi^4 r^4}{120} + ...\right), \ [45] \tag{6.50}$$

where ρ_0 is the galactocentric density, ρ_0^{NFW} is related to the density of the universe at the moment the halo collapsed and r_0, r_S, r_c are core, scale, characteristic radii respectively, while $\xi = \sqrt{Gm^3/\hbar^2 a}$ in which m is the mass of the dark matter particle and a is the scattering length [45]. The fitted latest data on Milky Way dark matter central density are $\rho_0^{BP} = 4.13 \times 10^7\ M_{\odot}{\rm kpc}^{-3}$ (Burkert profile) and $\rho_0^{NFW} = 1.40 \times 10^7\ M_{\odot}{\rm kpc}^{-3}$ (NFW profile) [56]. In both cases, we see that these fitted values are four

orders of magnitude *less* than $\rho_{0,\mathrm{MW}}^{\mathrm{upper}}$, as desired. From Eq.(6.46), for $\alpha \sim 7.68$, we get $\rho_{0,\mathrm{MW}}^{\mathrm{lower}} \sim 2.09 \times 10^3\ M_\odot \mathrm{kpc}^{-3}$ and $\langle\rho\rangle_{0,\mathrm{MW}}^{\mathrm{lower}} \sim 6.37 \times 10^2\ M_\odot \mathrm{kpc}^{-3}$. Once again, we see that the densities satisfy $\rho_0^{\mathrm{lower}} < \rho_0^{BP,\ NFW} < \rho_0^{\mathrm{upper}}$. A larger value of α does not disallow the inequalities at either end.

Apart from the galactocentric density ρ_0, the local (at $R_\odot = 8.5$ kpc) dark matter density $\rho_\odot$ provides a strong basis for the experimental endeavors for indirect detection of the dark matter. Though there is broad consensus, different groups have come up with somewhat different conclusions regarding the local density of dark matter. For example, Kuijken and Gilmore [41] find a volume density near Earth $\rho_\oplus \simeq 0.01$ GeV/cm$^3 = 2.64 \times 10^5\ M_\odot \mathrm{kpc}^{-3}$. Other reported values are the following: Bahcall *et al.* [57] find a best-fit value of $\rho_\odot = 0.34$ GeV/cm$^3 = 8.96 \times 10^6\ M_\odot \mathrm{kpc}^{-3}$, Caldwell and Ostriker [58] find $\rho_\odot = 0.23$ GeV/cm$^3 = 6.07 \times 10^6\ M_\odot \mathrm{kpc}^{-3}$, while Turner [59] calculates $\rho_\odot = 0.3 - 0.6$ GeV/cm$^3 = 7.92 \times 10^6 - 1.58 \times 10^7\ M_\odot \mathrm{kpc}^{-3}$. For a more comprehensive discussion on the distribution of dark matter, see [60]. The local dark matter energy density, consistent with standard estimates, is $\rho_\odot = (0.3 \pm 0.1)$ GeV/cm$^3 = 7.92 \times 10^6\ M_\odot \mathrm{kpc}^{-3}$ [61]. Bergstrom, Ullio and Buckley [62] find local dark matter densities acceptable in a somewhat broad range $0.2 - 0.8$ GeV/cm^3. The fitting with Burkert profile yields $\rho_\odot^{BP} = 0.487$ GeV/cm$^3 = 1.28 \times 10^7\ M_\odot \mathrm{kpc}^{-3}$ and fitting with NFW profile yields $\rho_\odot^{NFW} = 0.471$ GeV/cm$^3 = 1.24 \times 10^7\ M_\odot \mathrm{kpc}^{-3}$ [56]. About systematic uncertainties in the determination of local density of dark matter, see [63]. Overall, one could fairly say that $\rho_\odot \propto 10^6 - 10^7\ M_\odot \mathrm{kpc}^{-3}$.

We use the above local values as a constraint to estimate the central density ρ_0^{BEC} given in Eq.(6.50) that approaches a constant value ρ_0^{BEC} as $r \to 0$ (so does the EiBI profile $\rho^{(0)}(r)$ in Eq.(6.13) as the two are essentially of the same form). This behavior is consistent with the currently favored core behavior at the galactic center, as opposed to the NFW cusp. To estimate the values of ρ_0^{BEC} for the Milky Way, we constrain the BEC profile such that it coincides with the local value $\rho_\odot^{BP} = 1.28 \times 10^7$ $M_\odot \text{kpc}^{-3}$ at $R_\odot = 8.5$ kpc (boundary condition). This then yields a central density $\rho_0^{BEC} = 1.29 \times 10^7$ $M_\odot \text{kpc}^{-3}$. This is quite an acceptable central density value for the Milky Way. (We could as well use the same boundary condition using $\rho_\odot^{NFW}$, but it does not lead to a much different value for ρ_0^{BEC}). Having determined the value of ρ_0^{BEC}, we compare it with the corresponding values from NFW and Burkert profiles using data from [56] and observe the following: (i) ρ_0^{BEC} is quite comparable with ρ_0^{BP} and ρ_0^{NFW}, (ii) the NFW cusp and the PI, Burkert core behavior are evident from Figure 6.6. (iii) Identifying the BEC constant $\xi \equiv \frac{\pi}{R_{\text{DM}}}$, we see that the ρ^{BEC} profile shows a *much slower* monotonic decline from its central value ρ_0^{BEC}, coasting along almost flat all the way up to a finite R_{DM} (= 111.90 kpc, in the present case), where it vanishes, (iv) adopted values from the Burkert profile has allowed us to predict ρ_0^{BEC}, which is seen also to be included in the limiting interval, $\rho_0^{\text{lower}} < \rho_0^{BEC,BP,NFW} < \rho_0^{\text{upper}}$ for the Milky Way.

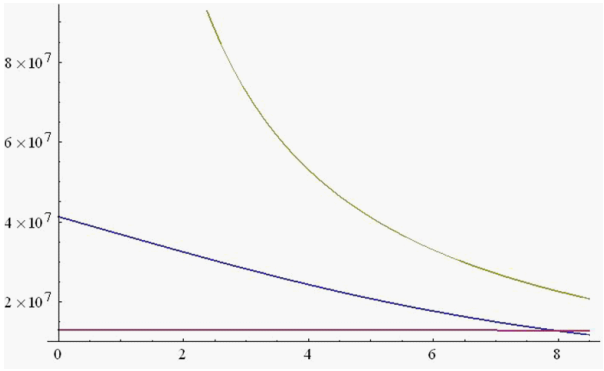

Figure 6.6. Plot of $\rho(r)$ vs r for three profiles for the Milky Way. The bottom one is for th -e BEC profile($\rho_0^{BEC} = 1.292 * 10^7 M_\odot\ kpc^{-3}$, $\xi = \frac{\pi}{R_{DM}} = 0.028$ kpc^{-1}), the middle one is due to Burkert profile ($\rho_0^{BP} = 4.13 * 10^7\ M_\odot\ kpc^{-3}$, $r_0 = 9.26$ kpc), the upper most curve represents NFW profile($\rho_0^{NFW} = 1.40 * 10^7\ M_\odot\ kpc^{-3}$, $r_s = 16.1kpc$). Data taken from [56].

Returning to the profiles (6.49) and (6.50), it is remarkable that the PI and BEC profiles have the same behavior up to second order in r provided we identify $r_c = \frac{\sqrt{6}}{\xi}$ but they begin to differ in the higher order coefficients thereafter. Also, it is known that the large majority of the high-resolution rotation curves prefer the PI core-dominated halo model, which provide a better description of the data than the cuspy ($\rho^{NFW} \propto r^{-1}$) NFW profile [64]. In this sense, the EiBI model could be a competing candidate to PI model. It would be our future task to investigate where these two models agree and where they disagree.

6.7 Discussion

The present chapter, based on a pivotal input from Weyl gravity, viz., $R_{\rm DM} = R_{\rm WR}$ (motivated by [16]), offers a new alternative *analytical* window, different from the standard data-fit approaches, to look at the physical galactic parameters. Our present discussion showed that how can we make a quantitative predictions about the limits on central dark matter density ρ_0. Many samples for which the values of ρ_0 are available are shown to satisfy the inequality $\rho_0 \leq \rho_0^{\rm upper} \propto R_{\rm WR}^{-2} \sim 10^{12}\ M_\odot {\rm kpc}^{-3}$. Only some samples are tabulated here.

Going a step further, we also calculated $\rho_0^{\rm lower} \propto (\alpha - 1) M_{\rm lum} R_{\rm WR}^{-3}$ that depends on a certain parameter α equal to the ratio of luminous to total (dark matter included) mass of a galaxy. Definitive estimates of such ratios are yet unavailable. Nevertheless, it is shown that (Table II), for reasonably wider values of α (≥ 12.5) accounting for

huge quantities of dark matter in individual samples, profile dependent values of ρ_0 still fall inside the EiBI predicted interval $\rho_0^{\rm lower} \leq \rho_0 \leq \rho_0^{\rm upper}$. These limits cover a large class of galaxies and indicate an interesting facet of the EiBI theory. We especially point out that the maximal value $\rho_0^{\rm upper} \propto R_{\rm WR}^{-2} \sim 10^{12}\ M_\odot{\rm kpc}^{-3}$ is purely a stability induced constraint on all galaxies with dark matter, while $(\alpha-1)M_{\rm lum}R_{\rm WR}^{-3}$ $\propto \rho_0^{\rm lower} \leq \rho_0$ is not, due to uncertainties in α. Thus, we would particularly advocate a practical verification of $\rho_0^{\rm upper}$ $(\propto 1/\kappa)$ rather than $\rho_0^{\rm lower}$. If verified, it would also mean that we have a clear-cut theoretical algorithm, applicable to all galactic samples, that provides a definitive, falsifiable information on the radius $R_{\rm DM}$ of dark matter/halo − something that seems rather scarce in the astrophysical literature.

A special merit of the foregoing analyses is that the only information needed to calculate the above limits are those of the fitted luminous $M_{\rm lum}$ values and the measured total mass $M_{\rm tot}$. Note that a small change in $M_{\rm lum}$ would lead to a large change in $R_{\rm WR}$. For instance, there is an argument [44, 65] for an upper mass limit indicated by the sudden decline of the visible baryonic mass function of disk galaxies at $M_{\rm disc}^{\rm max} = 2\times 10^{11}M_\odot$. Tentatively assuming that the luminous part of the Milky Way mass $M_{\rm lum}$ is $2\times 10^{11}M_\odot$ instead of $1.04\times 10^{11}M_\odot$, then the resultant $R_{\rm WR}$ would jump to 177.94 kpc from 111.90 kpc. Similarly, $R_{\rm term}$ would jump to 238 kpc from 150.17 kpc. Thus, for reliable values of $R_{\rm WR}$, the luminous mass data $M_{\rm lum}$ should be as accurate as possible.

We have verified that quantitative upper limit $\rho_0^{\rm upper} \sim 10^{12}\ M_\odot{\rm kpc}^{-3}$ is respected

by all the samples collected in [37], some of which are given in Table II. The reason for such consistency is not accidental – it stemmed from the fact that the Weyl radius $R_{\rm WR}$ has a solid foundation: The rotation curve is a *prediction* of Weyl gravity MO solution containing constants (γ_0, γ^*, k) that are universally applicable to all the galaxies, LSB or HSB, and that the $R_{\rm WR}$ is a straightforward result from $V'' < 0$. In fact, the reported data on $R_{\rm last}$ for individual samples have so far been found to obey $R_{\rm last} < R_{\rm WR}$. So we conjectured that this radius $R_{\rm WR}$ just might be *the* dark matter radius $R_{\rm DM}$ specific to individual galaxies.

As we saw, the constraint $\rho_0 \leq \rho_0^{\rm upper} \sim 10^{12}\ M_\odot{\rm kpc}^{-3}$ is a necessary condition for stability of circular orbits. Whether it is also a sufficient condition, that is, whether there are no stable orbits in the halo if this constraint is violated, is a matter of independent practical verification. If sufficiency turns out to be true, then we might expect to observe galaxies with no information on dark matter due to lack of stable circular orbits. It may be noted that our $\rho_0^{\rm upper} \sim 6.14 \times 10^{11}\ M_\odot{\rm kpc}^{-3}$ for Milky Way is remarkably consistent with the *local upper limit* on the dark matter density in the solar system, $\rho_\odot^{\rm upper} \sim 2.94 \times 10^{12}\ M_\odot{\rm kpc}^{-3}$, found by completely different methods and ideas [66].

There are limitations with almost all well known density profiles in the sense that they fit the data so well in one sector, but fail in the other. For instance, it has been argued [67] that the NFW profile does not always follow from the gas rotation curves of large samples. For a constant velocity anisotropy, the PI profile is ruled out,

while a truncated flat (TF) model [68] and NFW model are consistent with the data. Incidentally, it might be noted that the TF model expands up to r^2 like both in the PI and BEC profiles, and further, like the MO model, TF is described solely by two parameters, mass and the scale length. Nesti and Salucci [56] argue that NFW and/or PI halos are not supported by present day observations in external galaxies due to recent improvement of simulation techniques. URC profile for velocity distribution seems to fit the data incredibly well up to $\sim$ 30 kpc [24]. The present model based on EiBI Eq.(6.13), which is akin to the quantum BEC model, is probably no better or worse than the others. Nevertheless, the foregoing study hopefully provides some new definitive information in an analytic way using a metric solution (6.18) of EiBI theory.

Table I

Galaxy $\alpha = 12.5$	$R_{\rm WR}$ (kpc)	$R_{\rm term}$ (kpc)	κ $(\rm kpc)^2$	$\langle\rho\rangle^{\rm lower}$ $(M_\odot \rm kpc^{-3})$	γ	$\beta = \alpha\gamma$
ESO1870510	39.66	52.96	318.83	$2.45 * 10^4$	1.62	20.25
ESO3020120	44.77	60.15	406.11	$1.71 * 10^4$	1.07	13.37
ESO3050090	39.45	52.65	315.37	$2.49 * 10^4$	0.32	04.00
ESO4880490	42.25	56.62	361.70	$2.03 * 10^4$	3.07	38.37
U04115	39.02	52.03	308.53	$2.58 * 10^4$	0.97	12.12
U11557	41.75	55.91	353.21	$2.11 * 10^4$	0.20	02.50
U11748	106.18	142.57	2284.84	$1.28 * 10^3$	0.40	05.00
U11819	72.80	98.08	1073.95	$3.97 * 10^3$	2.24	28.00
U11583	39.08	52.11	309.47	$2.57 * 10^4$	0.70	08.75
F568-3	50.10	67.53	508.76	$1.22 * 10^4$	4.2	52.50
F583-1	41.50	55.57	349.11	$2.14 * 10^4$	1.6	20.00

Table II

(All densities are in units of $M_{\odot}\mathrm{kpc}^{-3}$)

Galaxy $\alpha = 12.5$	ρ_0^{lower}	ρ_0^{BEC}	ρ_0^{PI}	ρ_0^{NFW}	ρ_0^{upper}
ESO 1870510	$8.08 * 10^4$	$3.29 * 10^7$	$5.48 * 10^7$	$7.61 * 10^5$	$4.88 * 10^{12}$
ESO 3020120	$5.63 * 10^4$	$2.29 * 10^7$	$5.98 * 10^7$	$2.65 * 10^6$	$3.83 * 10^{12}$
ESO 3050090	$8.22 * 10^4$	$2.17 * 10^7$	$2.76 * 10^7$	$3.28 * 10^7$	$4.93 * 10^{12}$
ESO 4880490	$6.69 * 10^4$	$5.49 * 10^7$	$1.03 * 10^8$	$1.42 * 10^6$	$4.30 * 10^{12}$
U04115	$8.49 * 10^4$	$1.43 * 10^8$	$1.51 * 10^8$	$1.39 * 10^5$	$5.04 * 10^{12}$
U11557	$6.94 * 10^4$	$4.69 * 10^9$	$1.57 * 10^7$	$1.08 * 10^4$	$4.41 * 10^{12}$
U11748	$4.21 * 10^3$	$4.20 * 10^8$	$1.67 * 10^9$	$2.04 * 10^8$	$6.81 * 10^{11}$
U11819	$1.30 * 10^3$	$5.39 * 10^7$	$8.69 * 10^7$	$1.19 * 10^6$	$1.45 * 10^{12}$
U11583	$8.45 * 10^4$	$9.53 * 10^7$	$1.19 * 10^8$	$1.36 * 10^5$	$5.03 * 10^{12}$
F568-3	$4.01 * 10^4$	$2.48 * 10^7$	$3.61 * 10^7$	$3.78 * 10^5$	$3.06 * 10^{12}$
F583-1	$7.05 * 10^4$	$1.90 * 10^7$	$3.17 * 10^7$	$3.45 * 10^5$	$4.46 * 10^{12}$

References

[1] O. Bertolami, C. G. Boehmer, T. Harko and F. S. N. Lobo, Phys. Rev. D **75**, 104016 (2007).

[2] T. Harko and F. S. N. Lobo, Eur. Phys. J. C **70**, 373 (2010).

[3] A. S. Eddington, The mathematical theory of relativity, (Cambridge University Press, Cambridge, 1924).

[4] M. Born and L. Infeld, Proc. R. Soc. A **144**, 425 (1934).

[5] M. Banados and P. G. Ferreira, Phys. Rev. Lett. **105**, 011101 (2010).

[6] Paolo Pani, Vitor Cardoso, and Terence Delsate, Phys. Rev. Lett. **107**, 031101, July 2011.

[7] P. P. Avelino and R. Z. Ferreira, Phys. Rev. D **86,** 041501(R), 2012.

[8] Paolo Pani, T. Delsate and V. Cardoso, Phys. Rev. D **85**, 084020, 2012.

[9] Hyeong Chan Kim, Journals of the Korean Physical Society, Vol-65, Issue 6, pp 840-845, sept, 2014.

[10] J. H. C. Scargill, M. Banados and P. G. Ferreira, Phys. Rev. D **86**, 103533 (2012).

[11] P. Pani and T. P. Sotiriou, Phys. Rev. Lett. **109**, 251102 (2012).

[12] X.-L. Du, K. Yang, X.-H. Meng and Y.-X. Liu, Large Scale Structure Formation in Eddington-inspired Born-Infeld Gravity, Phys. Rev. D **90,** 044054 (2014).

[13] Y.-X. Liu, K. Yang, H. Guo and Y. Zhong, Domain Wall Brane in Eddington Inspired Born-Infeld Gravity, Phys. Rev. D **85**, 124053(2012).

[14] Q.-M. Fu, L. Zhao, K. Yang, B.-M. Gu and Y.-X. Liu, Stability and (quasi)localization of gravitational fluctuations in an Eddington-inspired Born-Infeld brane system, Phys. Rev. D **90,** 104007 (2014).

[15] S.-W. Wei, K. Yang and Y.-X. Liu, Black hole solution and strong gravitational lensing in Eddington-inspired Born-Infeld gravity, Eur. Phys. J. C **75** (2015) 253.

[16] A. Edery and M.B. Paranjape, Classical tests for Weyl gravity: Deflection of light and radar echo delay, Phys. Rev. D **58,** 024011(1998).

[17] A. Bhattacharya, A. Panchenko, M. Scalia, C. Cattani and K.K. Nandi, Light bending in the galactic halo by Rindler-Ishak method, JCAP **09**, 004 (2010).

[18] A. Bhattacharya, G.M. Garipova, E. Laserra, A. Bhadra and K.K. Nandi, The Vacuole Model: New Terms in the Second Order Deflection of Light, JCAP **02**, 028 (2011).

[19] D. Cutajar and K.Z. Adami, Strong lensing as a test for Conformal Weyl Gravity, Mon. Not. Roy. Astron. Soc. **441**, 1291(2014).

[20] F. Rahaman, K.K. Nandi, A. Bhadra, M. Kalam and K. Chakraborty, Perfect Fluid Dark Matter, Phys. Lett. B **694,** 10 (2010).

[21] T. Harko and F.S.N. Lobo, Two- fluid dark matter models, Phys.

Rev. D **83**, 124051(2011).

[22] T. Harko, F.S.N. Lobo, M.K. Mak and S.V. Sushkov, Dark matter density profile and galactic metric in Eddington-inspired Born-Infeld gravity, Mod. Phys. Lett. A **29**, 1450049 (2014).

[23] P. Pani, T. Delsate and V. Cardoso, Eddington-inspired Born-Infeld gravity. Phenomenology of non-linear gravity-matter coupling, Phys. Rev. D **85**, 084020 (2012).

[24] P. Salucci and A. Burkert, Dark matter scaling relations, Astrophys. J. **537,** L9 (2000).

[25] P. Salucci and M. Persic, Maximal halos in high-luminosity spiral galaxies, Astron. Astrophys. **351,** 442 (1999).

[26] K.K. Nandi, A.I. Filippov, F. Rahaman, S. Ray, A.A. Usmani et al., Features of galactic halo in a brane world model and observational constraints, Mon. Not. Roy. Astron. Soc. **399**, 2079 (2009).

[27] P.D. Mannheim and J.G. O'Brien, Impact of a global quadratic potential on galactic rotation curves, Phys. Rev. Lett. **106,** 121101 (2011).

[28] K.K. Nandi and A. Bhadra, Comment on 'Impact of a Global Quadratic Potential on Galactic Rotation Curves', Phys. Rev. Lett. **109,** 079001 (2012).

[29] K. Lake, Galactic potentials, Phys. Rev. Lett. **92,** 051101 (2004).

[30] M. Baiiados and P.G. Ferreira, Eddington's theory of gravity and

its progeny, Phys. Rev. Lett. **105,** 011101 (2010).

[31] S. Deser and G.W. Gibbons, Born-Infeld-Einstein actions, Class. Quant. Grav. **15,** L35 (1998).

[32] P. P. Avelino, Phys.Rev. D **85,** 104053, 2012.

[33] Soumya Jana and Sayan Kar, Phys. Rev. D **88**, 024013 (2013).

[34] S. Chandrasekhar, An introduction to the study of stelllar-structure, New York, Dover Publications (1957).

[35] G. P. Horedt, Polytropes: applications in astrophysics and related fields, Dordrecht, Boston, Kluwer Academic Publishers (2004).

[36] Alexander A. Potapov et al., Constraint on dark matter central density in the Eddington inspired Born-Infeld (EiBI) gravity with input from Weyl gravity, JCAP **07**, 018 (2015).

[37] P.D. Mannheim and J.G. O'Brien, Phys.Rev. D **85**, 124020 (2012).

[38] P. D. Mannheim, Prog. Part. Nucl. Phys. **56**, 340 (2006).

[39] R. H. Sanders, Astrophys. **J. 473**, 117 (1996).

[40] D. Lynden-Bell and G.Gilmore, eds., *Baryonic Dark Matter* (Kluwer, Dordrecht), 1990.

[41] K. Kuijken and G. Gilmore, Mon. Not. R. Astron. Soc. **239**, 571 (1989); *ibid.* **239**, 571 (1989); *ibid.* **239**, 605 (1989); *ibid.* **239**, 651 (1989); Astrophys. J. **367**, L9 (1991).

[42] W.J.G. de Blok and S.S. McGaugh, Mon. Not. Roy. Astron. Soc.

290, 533 (1997).

[43] A. Burkert, Astrophys. J. **447**, L25 (1995).

[44] P. Salucci *et al.* Mon. Not. R. Astron. Soc. **378**, 41 (2007).

[45] H. Robles and T. Matos, Mon. Not. R. Astron. Soc. **422**, 282 (2012).

[46] K.G. Begeman, A.H. Broeils and R.H. Sanders, Mon. Not. R. Astron. Soc. **249**, 523 (1991).

[47] J.F. Navarro, C.S. Frenk and S.D.M. White, Astrophys. **J. 462**, 563 (1996); ibid. **490**, 493 (1997).

[48] P. R. Kafle, S. Sharma, G.F. Lewis and J. Bland-Hawthorn, On the Shoulders of Giants: Properties of the Stellar Halo and the Milky Way Mass Distribution, Astrophys. J. **794**, 59 (2014).

[49] S.M. Faber and J.S. Gallaghar, Ann. Rev. Astron. Astrophys. **17**, 135 (1979).

[50] P.J. McMillan, Mon. Not. R. Astron. Soc. **414**, 2446 (2011).

[51] F. Iocco, M. Pato, G. Bertone and P. Jetzer, JCAP **11,** 029 (2011).

[52] V. Belokurov, N.W. Evans and J.H. An, Mon. Not. R. Astron. Soc. **424**, L44 (2012); A.J. Deason et al., Mon. Not. R. Astron. Soc. **425**, 2840 (2012).

[53] L.E. Strigari, Phys. Rep. **531**, 1 (2013).

[54] G. Bertone, D. Hooper and J. Silk, Phys. Rep. **405**, 279 (2005). It is an excellent and comprehensive review of the particle candidates

of dark matter.

[55] J.I. Read, J. Phys. G: Nucl. Part. Phys. **41**, 063101 (2014).

[56] F. Nesti and P. Salucci, JCAP **07,** 016 (2013).

[57] J. N. Bahcall, M. Schmidt and R. M. Soneira, Astrophys. J. **265**, 730 (1983).

[58] R. R. Caldwell and J. P. Ostriker, Astrophys. **J. 251**, 61 (1981).

[59] M. S. Turner, Phys. Rev. D **33**, 889 (1986).

[60] G. Jungman, M. Kamionkowski and K. Griest, Phys.Rept. **267**, 195 (1996).

[61] J. Bovy and S. Tremaine, Astrophys. **J. 756**, 89 (2012).

[62] L. Bergstrom, P. Ullio and J. H. Buckley, Astropart. Phys. **9**, 137 (1998).

[63] M. Pato, O. Agertz, G. Bertone, B. Moore, R. Teyssier, Phys. Rev. D **82**, 023531 (2010).

[64] W.J.G. de Blok, S.S. McGaugh and V.C. Rubin, Astron. **J. 122**, 2396 (2001).

[65] P. Salucci and M. Persic, Mon. Not. R. Astron. Soc. **309**, 923 (1999).

[66] L. Iorio, JCAP, **05,** 018 (2010).

[67] G. Battaglia et al., Mon. Not. R. Astron. Soc. **364**, 433 (2005).

[68] M. Wilkinson and N.W. Evans, Mon.Not.R.Astron.Soc. **310**, 645(1999).